Progressive damage modelling of RC columns under biaxial reverse cyclic load

Edel Martinez[1], Hugo Rodrigues[2], Humberto Varum[3], Solomon Tesfamariam[1]

[1] Ph.D. Student, School of Engineering, The University of British Columbia, Okanagan Campus, BC, Canada.
[2] Assistant Professor, RISCO – School of Technology and Management, Polytechnic Institute of Leiria, Portugal.
[3] Professor, CONSTRUCT – LESE, Department of Civil Engineering, Faculty of Engineering, University of Porto, Portugal.
[4] Professor, School of Engineering, The University of British Columbia, Okanagan Campus, BC, Canada.

ABSTRACT

In the present paper the problem of non-linear numerical modelling of highly localized deformation phenomena in reinforced concrete (RC) columns subjected to axial load and uni(bi)-directional cyclic lateral loads is analyzed. Simulations in uniaxial and biaxial loading are performed over different load paths. The finite element model was implemented in order to determine the global structural response and to capture locally damage mechanisms and failure modes, such as the crack opening-closure phenomena and yielding of reinforcing steel bars. To achieve that the concrete damaged plasticity model and a trilinear elastic-plastic steel model was considered in the refined modelling. The evaluated parameters were calibrated to the control of the damage evolution, based on degradation relationships of the energy dissipation capacity and ductility of RC columns. The predictive capability of the numerical approach was verified with experimental data. The discussion of results leads to a better understanding of global and local non-linear response mechanisms in RC structures under seismic loads.

Keywords: bidirectional horizontal cyclic demand, nonlinear numerical model, plastic hinge, local damage, model calibration.

INTRODUCTION

Reinforced concrete (RC) column under biaxial cyclic load has complex non-linear hysteretic response [1]. Non-linearity of the material can be affected by time-dependent viscous damping mechanisms [2]. Moreover, structures under seismic loads develop a deformed geometrical configuration and behave like a non-linear kinematic mechanism [3]. Damage mechanisms on the concrete and reinforcing steel includes concrete tensile cracking, crushing and spalling of concrete cover, pinching effects, and yielding and buckling of steel reinforcement. Moreover, failures of the RC columns might trigger progressive collapse [4, 5]. Although, columns are predominantly subjected to axial compression loads, under seismic loads, they are subjected to multi-axial reversed cyclic. Under reversed cyclic loading, special considerations must be taken as multidirectional and unrecoverable deformations are developed. However, such singularities are not easy to predict neither experimentally nor numerically.

This challenging topic has recently received special attention. Under biaxial analysis of the RC columns, inelastic deformation regimes can significantly affect the capacity of the member to dissipate energy and on its ductility [6]. This is described by higher stiffness and strength degradation and the observation of different failure patterns. Moreover, the performance of columns is affected by the load history and damage mechanisms, damage evolution, and failure patterns. Yu et al. [7], had stressed that the axial load ratio has also influence in the hysteric behavior of RC columns. However, bending analysis due to cyclic loading has been frequently oversimplified. There is a paucity of evidence to the correlation of multiaxial seismic loads. The consideration of the material behavior that accurately capture the damaged model under biaxial cyclic conditions has also received scant attention. The biaxial problem has received significant effort in experimental methods [8, 9]. A notable contribution was given by Nojavan et al. [10], who investigated the behavior of columns with large cross sectional dimensions and an ultra-high-performance fiber-reinforced concrete (UHP-FRC) under different loading protocols. Requirements for external strengthening and retrofitting of damaged RC columns has also encouraged researchers. Two examples of these applications are the use of carbon fiber-reinforced polymer [11] and steel-polypropylene hybrid fiber RC [12]. Overall, these experiments have addressed the problem under diverse considerations, for instance, the effect of the cross-section dimension, steel area ratio, load histories, comparative analysis with tests on uniaxial conditions, and variations in the axial load ratio. So far, however, there has been little discussion about the numerical analysis and constitutive modeling of RC columns under biaxial cyclic conditions. The mechanics that underpin the damage evolution of concrete constitutive models are not fully understood since the damage model proposed by Mazars and Pyaudier-Cabot [13]. Therefore, searching for a precise solution that combine cyclic loads is an urgent need, which require a complex formulation to be implemented. Consequently, it is required adjustments of the constitutive model to capture multiaxial stress-strain states [14].

Various methods for non-linear modeling of RC structures reported [e.g. 15-23]. Finite element analysis of fractured concrete was introduced by Maekawa et al. [15] in the smeared crack model (SCM). The SCM model and the discrete crack model are frequently used in modeling approaches. The former considers the strain localization phenomena in softening regime, thus, as explained by Bazant and Jaime [16], the crack propagation reduces the element size approaching a zero-energy dissipation and the results become mesh sensitive. The mesh sensitivity problem can be overcome using the crack band theory [17], where a fixed element size is related to the magnitude of fracture energy.

The approach given to problems to simulate columns in bending under the action of cyclic loads has been accomplished from a variety of models of concentrated inelasticity and distributed inelasticity, such as the lumped plasticity model. Distributed plasticity models allows a detailed analysis of nonlinearities associated with the inelastic response and has been successfully applied to RC structures by Huang and Kwon [18], where 320 experiments in RC columns were analyzed under quasi-static conditions. Also, RC columns under multiaxial conditions using a plasticity-distributed method have been modeled in OpenSees [11]. Member type models are also applied to the analysis of RC columns subjected bending moments. The model consider the non-linear behavior distributed in plastic hinges. The material properties of the sections located in the plastic hinge is responsible for the global behavior of the element. Scott and Fenves [19] proposed the numerical integration scheme for this model. Theoretically, local damage could be localized in sections outside the plastic hinge zone. The method fails to capture incremental inelastic distribution and cannot represent the actual damage pattern along the structural member. Despite these limitations, the method is able to predict with certain accuracy the hysteric response of RC members and generally low computational processing time is required. Fiber-section elements are used under the continuous section assumption. The section is discretized in fibers that characterized the uniaxial behavior of materials, concrete and reinforcing steel, and the longitudinal element is formulated under the concepts of beams theory of Euler-Bernoulli, Timoshenko, or generalized methods. The model was used to predict the behavior of RC columns subjected to biaxial cyclic loads [20]. In this method, transverse reinforcement is considered smeared and attributed to the concrete fibers of the section. Li et al. [21] proposed a 3D flexural-shear element implemented in a fiber-based model applied to RC columns subjected to biaxial bending moment. The method is suitable for applications in RC structures. Recent research attention has given to detailed finite element simulations of concrete members [18, 22-23], however, studies are still limited.

The present research is centered in assessment of detailed finite element analysis representing a group of experimental tests on cantilever RC column specimens under biaxial horizontal cyclic loading. This work intended to determine the effect of material parameters of the concrete damaged plasticity model (CDPM) on the damage evolution based on hysteric responses. Comparison of the overall response against experimental data confirms the accuracy of the solution. In addition, responses of inelastic local deformation based on damage mechanisms are captured, such as the cracking, yielding in reinforcing steel and penetrating yielding. The approach relies on the observation of damage evolution and plastic hinge regions in RC columns subjected to reversed cyclic.

EXPERIMENTAL CAMPAIGN

The data used in this study was tested at the Laboratory of Earthquake and Structural Engineering (LESE) at University of Porto [9]. The test is based on the assumption that corner columns in buildings of approximated 4 storey should reproduce multidirectional seismic excitations. Axial loading ratios were correspondingly applied. It is known that corner columns in gravity frames, despite not having large axial loads, would experience multidirectional seismic excitations. Tests were carried out on specimens subjected to an axial compression load constantly applied at the top while two actuators transmitted lateral loads on orthogonal directions under controlled displacement conditions. These actuators generated reversed moments at the base. Three cycles for each displacement demand were applied monotonically, and a stop criterion was established at the end of the third cycle to observe relevant features of the damaged specimen.

Four full-scale rectangular sections were considered. The specimens were classified into six series to reproduce effects on a variability of parameters, for instance, cross-section geometry, ratio of longitudinal reinforcing steel, material properties, uniaxial and biaxial conditions, axial load ratio, time history and the load paths. A total of 24 specimens of RC columns subject to cyclic lateral loads in one or two directions were tested. In this study, 4 specimens were selected to simulations, two in uniaxial conditions and two in biaxial conditions, as summarized in Table 1. The specimen height is consistent with a half double-curvature column of 3 m height and was added 0.20 m to support the actuators. Therefore, the specimen in cantilever is 1.70 m high and lateral loads are concentrated at 1.60 m height over the base. The clear height of the specimen is 1.50 m. The column specimen was cast on a strong foundation block with a square base of 1.30 m × 1.30 m and 0.50 m depth, which is fixed by 4 prestressed steel rods to the strong set-up floor. This avoided sliding and overturning at the base of the specimen during tests. Detailing of the reinforcing steel for the two considered cross-sections are shown in Figure 1(a).

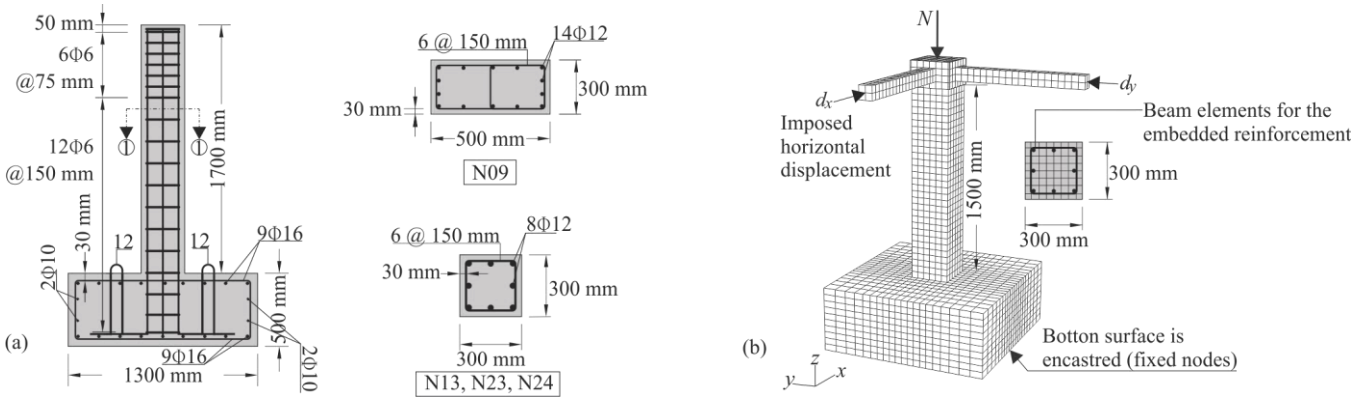

Figure 1. (a) Design dimension and reinforcing steel details of RC columns specimens. (b) Finite element model.

The square cross-section has 8 longitudinal reinforcement bars with a diameter of 12 mm and 6 mm diameter stirrups. The rectangular cross-section has 14 longitudinal steel bars with a diameter of 12 mm and 6 mm diameter stirrups and crosstie bar. Stirrups are spaced at 75 mm in the specimen top region and 150 mm along the specimen and to the interior of the foundation block. A 3 cm concrete cover was considered along the column specimen. In the foundation block, a cage of reinforcing steels of 10 and 16 mm diameters were detailed. The axial load capacity $A_g f_c'$ of the column PB01-N09 is 3658.5 kN, for the PB01-N13 is 1953.0 kN, and for the columns PB12-N23 and PB12-N24 is 3267.0 kN. The corresponding applied axial loads are 8.2 % (PB01-N09), 10.7 % (PB01-N13), and 19.9 % (PB12-N23 and PB12-N24). The material properties of concrete and reinforcing steel are shown in Table 1. These values are the result of an extensive experimental work. The concrete compressive strength and tensile strength was determined at the same time of the tested columns. The yield strength of the reinforcing steel slightly varies between specimens, as specified in Table 1. However, the tested yield strength and ultimate strength of the reinforcing steel for all column specimens is superior than nominal values for the European steel grade S400.

Table 1. RC column cross-section, material properties and loading conditions.

Specimen (Column)	Cross-section	f_{cm} [MPa]	f_t [MPa]	f_{ys} [MPa]	f_{su} [MPa]	E_s [GPa]	ε_{su} [%]	Axial load [kN]	Displacement history
PB01-N09	30x50	24.39	2.57	429.69	551.08	203.46	22.40	300	N-S / x – dir.
PB01-N13	30x30	21.70	2.98	429.69	551.08	203.46	22.40	210	W-E / y – dir.
PB12-N23	30x30	36.30	3.24	450.26	576.92	189.53	20.39	650	Rhombus
PB12-N24	30x30	36.30	3.24	450.26	576.92	189.53	20.39	650	Quadrangular

CONSTITUTIVE MODEL

The characterization of concrete and steel is individually considered. The concrete damaged plasticity model (CDPM), available in ABAQUS, and an elastic-plastic model for the reinforcement are briefly presented in this section. The plastic characteristics of the CDPM include a yield function proposed by Lubliner et al. [24] and modified by Lee and Fenves [25]. The CDPM captures the non-linear behavior of concrete in tension and compression through material parameters that consider both non-recoverable deformations and stiffness degradation. The formulae implemented in the CDPM might be divided into four groups: damage variable, yield criterion, hardening/softening rule, and flow rule.

Uniaxial behavior of the concrete in the softening regime

The CDPM define the concrete behavior. Plasticity and damage evolution are implemented as functions of inelastic deformations that will develop crushing or tension deformations with consequently tensile cracking. The softening behavior of concrete is represented by expansive volumetric strain and is a macroscopic consequence of the evolution of micro-cracks. This phenomenon is called damage in the context of the CDPM [25]. The stiffness degradation due to this process is clearly observed in reversed cyclic concrete tests. Special care is required in the definition of the concrete stress-strain curve in softening ranges. The considered model for the uniaxial compression stress-strain curve is shown in Figure 2(a). The tension-compression relationship is initially defined by a parabolic segment given by the Hognestad parabola

$$\sigma_{cm} = f_{cm}\left[2\left(\frac{\varepsilon_c}{\varepsilon_0}\right) - \left(\frac{\varepsilon_c}{\varepsilon_0}\right)^2\right] \quad (1)$$

for which the peak compression strength f_{cm} obtained from tests is used, and a second segment defined for the confined and unconfined concrete follows the Kent-Park concrete model [26]. The stress-strain behavior for the concrete under tension is approached using the relationship proposed by Hordijk [27]. In the softening range is defined that the tensile stress σ_t,

responsible for the tensile fractures, is a function of the crack width w and the properties of the material maximum tensile strength f_{cm} and critical crack opening w_c.

$$\frac{\sigma_t}{f_{tm}} = \left[1 + \left(c_1 \frac{w}{w_c}\right)^3\right] e^{-c_2 \frac{w}{w_c}} - \frac{w}{w_c}(1 + c_1^3) e^{-c_2} \tag{2}$$

where,

$$f_{tm} = f_{ctk0,m} \left(\frac{f_{ck}}{f_{ck0}}\right)^{2/3} \tag{3}$$

It is known that the critical crack opening w_c is related to loss of tensile strength. This is a property of the material and is associated with the tensile strength and the fracture energy of concrete G_F,

$$w_c = 5.14 \frac{G_F}{f_{tm}} \tag{4}$$

The values of the constants $c_1 = 3.0$ and $c_2 = 6.93$ were obtained from the work of Hordijk [27] on tensile tests. It is worth to note that the fracture energy, which is the energy release rate, is size independent and that can be used as a material property. This can be determined according to the following expression

$$G_F = 0.073 f_{cm}^{0.18} \tag{5}$$

or using the CEB-FIP Model [28]

$$G_F = (0.0469 d_a^2 - 0.5 d_a + 26) \left(\frac{f_{tm}}{10}\right)^{0.7} \qquad [\mathrm{N/mm}] \tag{6}$$

where d_a is the maximum size of the aggregate used in the concrete. The crushing energy and the fracture energy are related in the following equation

$$G_{ch} = \left(\frac{f_{cm}}{f_{tm}}\right)^2 G_F \tag{7}$$

Finally, the expression used to reproduce the stress-strain curve based on the stress-fracture opening curve is

$$\varepsilon_t = \varepsilon_{tm} + \frac{w}{l_{eq}} \tag{8}$$

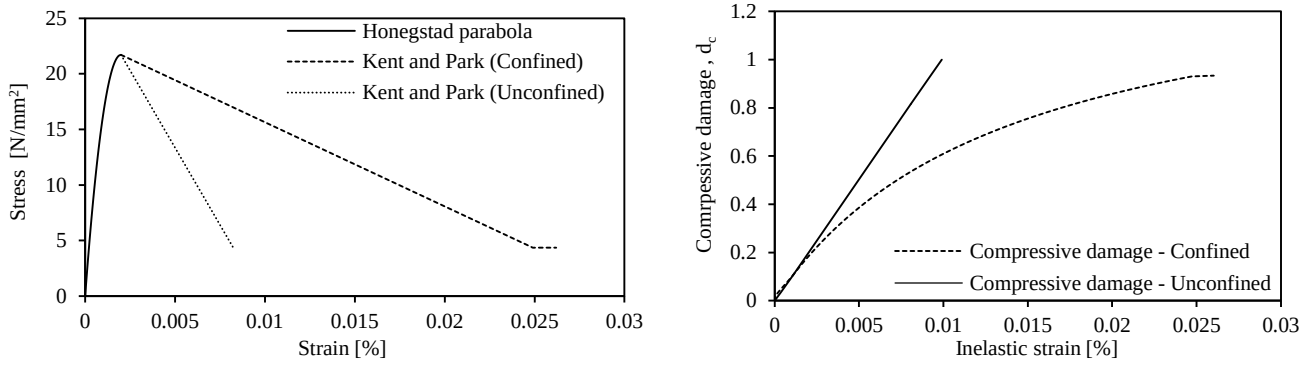

(a) (b)

Figure 2. (a) Uniaxial compressive stress-strain models; (b) compressive damage variable.

Concrete damaged plasticity model

Damage parameters were introduced to simulate damage evolution during compression (crushing) and tension (cracking). The CDPM requires strain data in uniaxial compression and tension conditions and consider biaxial stress conditions. The CDPM modify the failure surface of the Drucker-Prager criterion using the parameter K_c in the deviatoric cross section. The parameter K_c is define for a pressure invariant p as the ratio of distances between the hydrostatic axis and the tensile meridian (TM) and compression meridian (CM) in the deviatoric cross section. This parameter affects the failure surface and ranges between 0.5, which is a Rankine yield surface, to 1 for the Drucker-Prager hypothesis. The default value used in simulation is $K_c = 2/3$. Moreover, the model considers irreversible damage of the plain concrete. The plasticity characterizes irreversible deformations through the consideration of small deformations separated into elastic ε^e and plastic components ε^p, thus $\varepsilon = \varepsilon^e + \varepsilon^p$, where ε^{el} is the elastic strain the and ε^{pl} the plastic strain. Moreover, considering that the concrete is a quasi-brittle material vulnerable to damage evolution caused by inelastic deformations, a damage variable is introduced into the modelling. The CDPM considers the damage evolution in the cracked material, that is during the post-peak behavior typical of the plastic flow, introducing a scalar variable of damage d for multiaxial conditions, this value oscillates between zero and 1. For the uniaxial compression and tension behavior, when the elastic region terminates, softening governs the stiffness degradation, and computed as:

$$\sigma_{ij} = (1-d)D^{el}_{ijkl}\left(\varepsilon_{ij} - \varepsilon^{pl}_{ij}\right) \tag{9}$$

where σ_{ij} is a stress state function, D^{el}_{ijkl}, is the initial elasticity matrix, ε_{ij} is the tensor strain and ε^{pl}_{ij} is the tensor plastic strain. The parameter d evaluates uniaxial tension and compression, d_t and d_c, respectively. Simplifying equation (9) for each stress and compression damage parameter,

$$\sigma_t = (1-d_t)E_0\left(\varepsilon_t - \varepsilon^{pl}_t\right) \tag{10}$$

$$\sigma_c = (1-d_c)E_0\left(\varepsilon_c - \varepsilon^{pl}_c\right) \tag{11}$$

For uniaxial cyclic loading conditions, it is given as

$$d = 1-(1-s_t d_c)(1-s_c d_t) \tag{12}$$

where E_0 is the initial (undamaged) elastic modulus, s_c and s_t are parameters responsible for reproducing the unilateral effect associated with the reversed stresses; σ_c/σ_t, $\varepsilon_c/\varepsilon_t$, $\varepsilon^{pl}_c/\varepsilon^{pl}_t$ are resistance stresses, total deformations, plastic deformations for compression and tension, respectively. The damage parameters for the state of compression tension d_c or tension d_t characterize the evolution of the initial elastic stiffness degradation E_0 (undamaged) only after the material reaches the compressive and tensile deformations in the softening range. Damage variables were defined for the confined and unconfined concrete, as shown in Figure 2(b). The value of the damage parameter ranges from 0 to 1 for the undamaged to fully damaged state, respectively.

The elastic stiffness degradation at any instant of inelastic deformation is then generalized

$$E = (1-d)E_0 \tag{13}$$

$$1-d = (1-s_t d_c)(1-s_c d_t) \tag{14}$$

$$s_c = 1-h_c\left(1-r^*(\sigma_{11})\right) \tag{15}$$

$$s_t = 1-h_t r^*(\sigma_{11}) \tag{16}$$

where h_c and h_t are weighting factors ranging between 0 and 1. The deformations in the softening range of each curve separately to define crack strain ε^{in}_c and inelastic strain ε^{in}_c are defines as follows,

$$\varepsilon^{ck}_t = \varepsilon_t - \frac{\sigma_t}{E_0} \tag{17}$$

$$\varepsilon^{in}_c = \varepsilon_c - \frac{\sigma_c}{E_0} \tag{18}$$

The CDPM takes these deformations from the damage curves and determine plastic deformations through the relationships,

$$\varepsilon^{pl}_c = \varepsilon^{in}_c - \frac{d_c}{(1-d_c)}\frac{\sigma_c}{E_0} \tag{19}$$

$$\varepsilon^{pl}_t = \varepsilon^{ck}_t - \frac{d_t}{(1-d_t)}\frac{\sigma_t}{E_0} \tag{20}$$

The energy release rate G_f is the energy that is required to create a fracture area unit. This concepts is represented by g_c and g_t as the area below the softening range in the stress-strain curve. The compressive and tensile dissipative quantities g_c and g_t are proportional to the ratio between the fracture energies in compression G_c and tension G_t and the characteristics lengths L_c and tension L_t, that is $g_c = G_c/L_c$ and $g_t = G_t/L_t$.

The CDPM defines a non-associated potential flow rule, which is based on a Drucker-Prager hyperbolic function, of the form $G = \sqrt{(\epsilon\sigma_{t0}tan\psi)^2 + q^2} - ptan\psi$, where ϵ is the eccentricity of the plastic potential surface, σ_{t0} the uniaxial tensile stress at failure, and ψ the dilatation angle measured in the $p-q$ plane. The approach rate of the shape of the hyperbolic surface to its asymptote is given by the eccentricity ϵ. By definition, when the eccentricity tends to zero the flow potential becomes the classic case of Drucker-Prager. The recommended value for modeling through the CDPM is $\epsilon = 0.1$. On the other hand, the dilatation angle ψ, is a physical representation of the internal friction angle of the concrete. Generally, for concrete is found values of ψ in the range of 32° to 40°. Moreover, the CDPM considers failure on biaxial conditions. Based on this concept an state parameter of the material behavior is defined up to failure, which is a relationship of strengths between the biaxial state and uniaxial state σ_{b0}/σ_{c0}. From analyzes carried out in experimental investigations of the concrete strength was determined $\sigma_{b0}/\sigma_{c0} = 1.16$. As previous explained, the CDPM is verified through the four parameters, K_c, ψ, σ_{b0}/σ_{c0}, ϵ, for which the values used herein are summarized in Table 2.

Table 2. Parameters of the concrete damaged plasticity model.

K_c	Dilatation angle ψ [°]	σ_{b0}/σ_{c0}	Eccentricity ϵ
0.667	32	1.16	0.1

Reinforcing steel model

A tri-linear elastic-plastic curve with best fit to experimental results is used in this work. The linear-elastic stage of the model curve match the experimental data, with an slope equal to the modulus of elasticity of steel E_s and maximum value at the yield strength f_{sy}. The subsequent stage refers to the yield plateau. The last stage captures an isotropic strain-hardening in post-yield plastic regimes that ends at the ultimate strength f_u. The hardening stage is considered because the reinforcing steel highly contributes to the inelastic behavior of the column. Numerical values of the elastic segment, plateau segments, and ultimate strain are summarized in Table 1. The strain-hardening ratio assumed herein is 13.6 % in models with $\varepsilon_{su} = 22.4\%$ and 11.4% in models with $\varepsilon_{su} = 20.39\%$.

FINITE ELEMENT ANALYSIS

The solution scheme is based on non-linear dynamic simulations. The implicit integration algorithm was adopted to solve the dynamic equations of motion because it is unconditionally stable for time-step in a transient analysis. Simplified contact conditions between concrete-reinforcing steel were considered because the adopted solution scheme would present problems of convergence and impact on the computational time for complex interactions. The contact is simulated using the embedded technique available in ABAQUS [29]. Therefore, local bond slip effects are not considered, which implies perfect bond with no slip between the concrete and reinforcing steel. This is consistent with experimental observations, where no significant bond-slip effect was observed. Interactional effects are out of scope of this study, and methods including the effect of the rebar-concrete slippage under cyclic loading must be object of investigation. The model is approached in two and three dimensions. In three-dimensions, are used solid elements -8-node linear brick with reduced integration (C3D8R)- for concrete and 2-node linear beam (B31) for the reinforcement. In two-dimensions, the 4-node bilinear reduced integration with hourglass control (CPS4R) is used for the concrete and the B31 for the reinforcement. This strategy intends to perform a robust simulation and decrease the computational cost by simplifying uniaxial models. Local unrealistic damage of elements in contact with the actuators due to stress concentration is avoided using rigid brace elements. The actuator force is modeled as controlled displacements in reversed cyclic. The mesh generation, boundary constraints, and loading conditions for three-dimensional models is schematically represented in Figure 1(b). The generated mesh is regular and has mainly 50 mm size elements. The definition of a constant element size is required to determine the fracture energy G_f and minimize the inherent mesh sensitivity [30]. All nodes at the base were fully constrained. The model is loaded in three continuous steps. In the first step, gravity loads were imposed. Then, a constant axial load is applied at the top section at 10 kN per time increment, and it remains constant after the completion of the simulation. The last step is where lateral drift demand is applied by controlled displacements located at the top of the column. The specimen experience lateral drifts during 3 cycles for each displacement demand.

Hysteresis response of the model

This study has verified through modeling that the hysteresis behavior of the RC columns effectively takes into account the stiffness degradation. The simulations have reasonably good approximation of the stiffness degradation obtained in experiments. However, for large displacements, the model has a complex geometric non-linearity. The response becomes dependent of the magnitude of the displacement demand and abrupt changes in the load history were difficult to predict, as observed at the 'steps' of Figure 3(c) for the P12-N23 test. Figure 3(a) and (b) presents the hysteric behavior for tests on biaxial conditions. The results obtained in simulations super-estimate the initial stiffness but not the peak resistance. The main reason for this effect is that finite element analysis intrinsically predicts higher values of initial stiffness in the elastic phase.

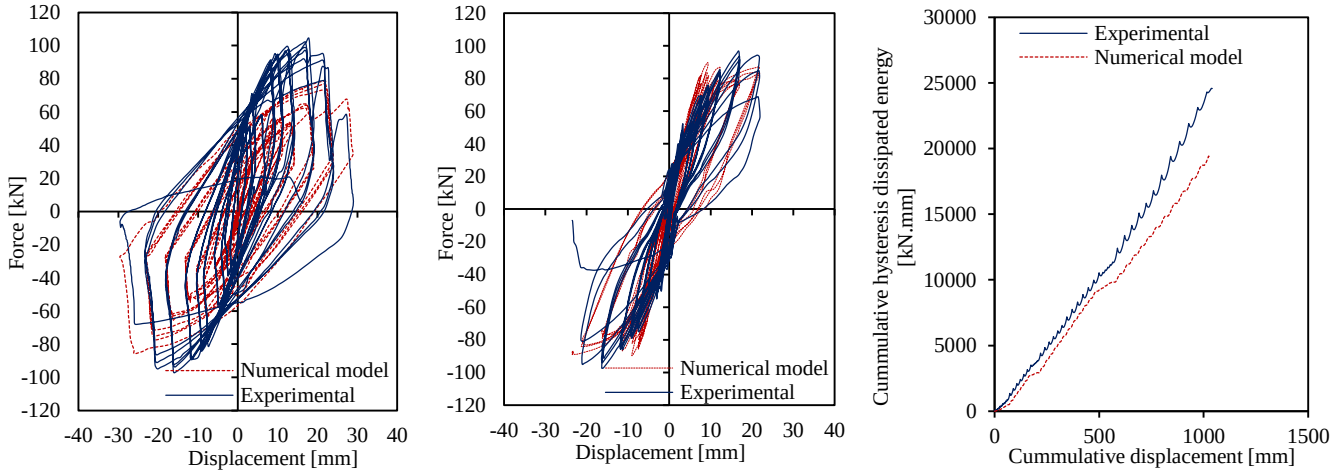

Figure 3. Force-deflection curve (a) PB12-N24 x-dir., (b) PB12-N23 y-dir., and (c) Energy dissipated by PB12-N23.

Energy dissipated

The energy dissipated is consequent of the accumulation of individual energies associated with the drift reached at each cyclic load amplitude, as represented in Figure 3(c). The energy dissipated due to cycle increments is equivalent to the area enclosed in each hysteresis loop. It is verified that the energy dissipated from columns of RC increases for higher values of axial load, and independently of the geometry of the section and reinforcing steel area. The ductility decreases with the increase of the loading rate. Overall, the model was affect by changes on low and high cycle demands, for which the damage variable coupled into the finite element model was unable to properly capture the dissipated energy, as observed in Figure 3(c).

Observed damage

The damaged region at the column base in terms of plastic strain magnitudes is shown in Figure 4. It is observed that the damage region is a non-lineal zone around the plastic hinge zone. The results indicate that the modeled damage approximates the experiment response with accuracy. The damage evolution and consequent failure of sections consider fractures in the concrete, yielding in the reinforcement, spalling of the concrete cover, and crushing of concrete core. Based on input properties and different failure modes observed, can be summarized that: (1) compression damage increase at the base and is observed for larger displacement demands, (2) the loading combination significantly affects the damage evolution and failure mechanism, (3) damage bands associated with tensile fractures are initiated at the base and developed in bands around the plastic hinge. When this singularity takes place, the increasing demand of inelastic deformations causes progressively damage around the base of the model, where the energy dissipates, and consequently the longitudinal bars undergo yielding. On simulations the predominant bending response produce transverse cracks. This highly reduce the axial and lateral load capacity of the columns. It is captured in the model the pinching effect. Pinching is associated with the local damage at the base of the column associated with a fragile failure of the concrete without confinement. Moreover, the ductility of the column is affected by yielding of longitudinal reinforcement, which is related to the peak lateral strength of the specimen, and the local damage at the base. The specimen failure is governed by the bending response.

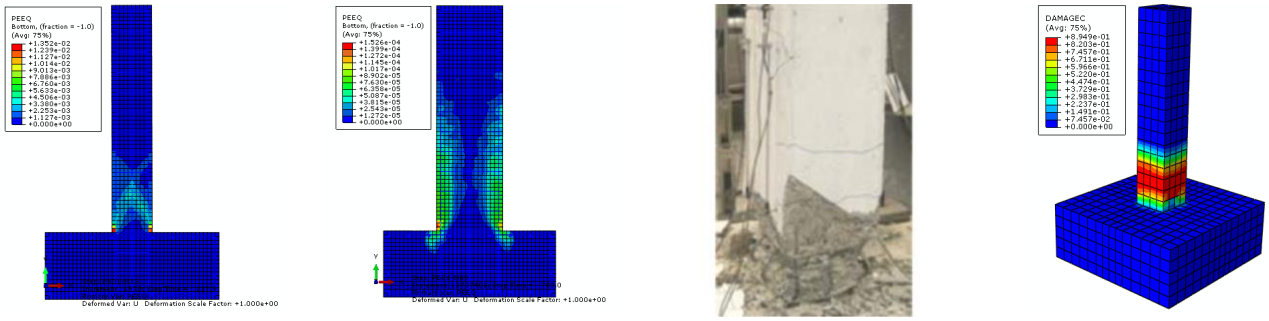

(a) (b) (c) (d)

Figure 4. Equivalent plastic strain magnitudes (a) PB01-N13 (b) PB01-N09. Damaged zone in PB12-N24 (c) test [9](d) model.

CONCLUSIONS

The constitutive approach used in this study is governed by the consideration of the damage evolution in RC columns subjected to reversal bending in biaxial cyclic conditions. Simulations demanded an important computational time but the results allowed a detailed visualization of the global response and to capture failure mechanisms and residual load capacity. The method addressed was verified against experimental data with good accuracy. This result will set up a framework for a solution of nonlinear problems of RC columns under biaxial cyclic loads. Based on the results obtained in this study the following specific conclusions can be drawn: (1) The response to biaxial cyclic loads produces more stiffness degradation for incremented cycles. This has important significance when evaluating compression members on structures subjected to earthquakes on the rigor imposed by current technical codes. (2) The damage analysis was mainly concentrated at the base of the column, in the plastic hinge zone. (3) The model provides the starting point and final size of plastic hinges, which is in agreement with the damage evolution described in experiments. It is recommended for future studies to take into account complex failure mechanisms of the reinforcing steel, for instance opening of stirrups and buckling of reinforcing longitudinal bars. Finally, the constitutive model should be verified over a wider range of biaxial stress states based on experimental data.

ACKNOWLEDGEMENT

The authors acknowledge the financial support through the Natural Sciences and Engineering Research Council of Canada (RGPIN-2014-05013) under the Discovery Grant programs, and Mitacs Accelerate program. The authors would like to acknowledge the technicians of the Laboratory of Earthquake and Structural Engineering (LESE), for their support in the experimental activity reported in this paper, and also to UID/ECI/04708/2019- CONSTRUCT - Instituto de I&D em Estruturas e Construções funded by national funds through the FCT/MCTES (PIDDAC).

REFERENCES

[1] Filiatrault, A., Tremblay, R., Christopoulos, C., Folz, B. and Pettinga., D. (2002). *Elements of Earthquake Engineering and Structural Dynamics*. 3rd ed. Presses Internationales Polytechnique, Canada.

[2] Saatci, S., and Vecchio, F.J. (2010). "Nonlinear finite element modeling of reinforced concrete structures under impact loads." *ACI Structural Journal*, 106, 717–726.

[3] Oller, S. (2001). *Nonlinear dynamics of structures: Lecture notes on numerical methods in engineering and sciences*. Springer International Publishing, Barcelona, Spain.

[4] Weng, J., Lee, C.K., Tan, K.H. and N.S. Lim. (2017). "Damage assessment for reinforced concrete frames subject to progressive collapse." *Engineering Structures*, 149, 147–160.

[5] Lu, X., Xinzheng, L, X., Hong, G., and Lieping, Y. (2013). "Collapse simulation of reinforced concrete high-rise building induced by extreme earthquakes." *Earthquake Engineering & Structural Dynamics*, 42, 705–723.

[6] Rodrigues, H., Arêde, A., Varum, H. and Costa, A. G. (2012). "Experimental evaluation of rectangular reinforced concrete column behaviour under biaxial cyclic loading." *Engng Struct. Dyn.*, 42, 239-259.

[7] Yu, J., Zhan, K., Li, L. and Yu, K. (2017). "Using XFEM to model the effect of different axial compression on the hysteretic behaviour of the flexure-dominant RC columns." *Struct. Design of Tall and Special Buildings*, 27(8), 1465.

[8] Wang, D., Li, H. and Li, G. (2013). "Experimental tests on reinforced concrete columns under multi-dimensional dynamic loadings." *Construction and Building Materials*, 47, 1167-1181.

[9] Rodrigues, H. (2012). *Biaxial seismic behaviour of reinforced concrete columns*. PhD thesis, University of Aveiro, Portugal.

[10] Nojavan, A., Schultz, A.E., Haselton, C., Simathathien, S., Liu, X. and Chao, SH. (2015). "A new dataset for full-scale RC columns under collapse-consistent loading protocols." *Earthquake Spectra*, 31(2), 1211–1231.

[11] Hashemi, M.J., Al-ogaidi, Y., Al-mahaidi, R., Kalfat, R. (2017). "Application of hybrid simulation for collapse assessment of post-earthquake CFRP-repaired RC columns." *Journal of Structural Engineering*, 143(1), 1–14.

[12] Chi, Y., Yu, M., Huang, L. and Xu, L.H. (2017). "Finite element modeling of steel-polypropylene hybrid fiber reinforced concrete using modified concrete damaged plasticity." *Engineering Structures*, 148, 23–35.

[13] Mazars, J., and Pyaudier-Cabot, G. (1989). "Continuum damage theory - application to concrete." *Journal of Engineering Mechanics*, 115(2), 345–365.

[14] Vecchio, F., and Collins, M. P. (1981). *Stress-strain characteristics of reinforced concrete in pure shear*. International Association for Bridge and Structural Engineering Colloquium, Final Report, University of Toronto, Canada.

[15] Maekawa, K., Irawan, P. and Okamura, H. (1997). "Path-dependent three-dimensional constitutive laws of reinforced concrete - formulation and experimental verifications." *Structural Engineering and Mechanics*, 5(6), 743–754.

[16] Bazant, Z.P., and Jaime, P. (1998). *Fracture and Size Effect in Concrete and Other Quasibrittle Materials.* 1st Edition.

[17] Bazant, Z.P., and Oh, B.H. (1983). "Crack band theory for fracture of concrete." *Matériaux Const.*, 16(93), 155-177.

[18] Huang, X. and Kwon, OS. (2015). "Numerical models of RC elements and their impacts on seismic performance assessment." *Earthquake Engineering & Structural Dynamics*, 44, 283–298.

[19] Scott, M.H., and Fenves, G.L. (2006). "Plastic hinge integration methods for force-based beam–column elements." *Journal of Structural Engineering*, 132(2), 244–252.

[20] Shirmohammadi, F., and Esmaeily, A. (2015). "Performance of reinforced concrete columns under bi-axial lateral force/displacement and axial load." *Engineering Structures*, 99, 63-77.

[21] Li, Z., Gao, Y. and Zhao, Q. (2016). "A 3D flexure – shear fiber element for modeling the seismic behavior of reinforced concrete columns." *Engineering Structures*, 117, 372–383.

[22] Lucchini, A., Franchin, P. and Kunnath, S. (2017). "Failure simulation of shear-critical RC columns with non-ductile detailing under lateral load." *Earthquake Engineering & Structural Dynamics*, 46(5), 855–874.

[23] Genikomsou, A.S., and Polak, M.A. (2015). "Finite element analysis of punching shear of concrete slabs using damaged plasticity model in ABAQUS." *Engineering Structures*, 98, 38–48.

[24] Lubliner, J., Oliver, J. Oller, S. and Oñate, E. (1989). "A plastic-damage model for concrete." *Int. J. Solids Structures*, 25(3), 299–326.

[25] Lee, J. and Fenves, G.L. (1998). "Plastic-damage model for cyclic loading of concrete structures." *Journal of Engineering Mechanics*, 124(8), 892–900.

[26] Kent, D. C. and Park, R. (1971). "Flexural members with confined concrete." *Journal of the Structural Division*, 97(7), 1969–1990.

[27] Hordijk, DA (1992). "Tensile and tensile fatigue behavior of concrete; experiments, modeling and analyses." *Heron*, 37(1). Stevin Laboratory, Delft University of Technology, Delft, The Netherlands.

[28] CEB (1991). *CEB-FIP Model Code 1990, Design Code*. Thomas Telford. London, England.

[29] Systèmes, D. (2014). "ABAQUS 6.14 Online Documentation." Providence, RI, USA.

[30] Bazant, Z.P. and Pijaudier-Cabot, G. (1988). "Nonlocal continuum damage, localization instability and convergence." *J. Appl. Mech.*, 55, 287–293.